Short communication: Field data imply that the sorting (D96/D50 ratios) of grains on fluvial gravel bars influences the probability of sediment entrainment

Running title: transport probability of coarse-grained material

Fritz Schlunegger, Romain Delunel and Philippos Garefalakis
Institute of Geological Sciences, University of Bern, 3012 Bern, Switzerland
+41 31 631 8767, schlunegger@geo.unibe.ch

Abstract

Conceptual models suggest that the mobility of grains on coarse-grained gravel bars is mainly controlled by sediment supply. Here we present field observations from streams in the Swiss Alps and the Peruvian Andes to document that for a given water runoff, the probability of material transport also depends on the sorting of the bed material. We calculate shear stresses that are expected for a mean annual water discharge, and compare these estimates with grain-specific thresholds. We find a positive correlation between the predicted probability of material transport and the sorting of the bed material, expressed by the D_{96}/D_{50} ratio. These results suggest that besides sediment supply, the bedload sorting exerts a measurable control on the mobility of clasts in coarse-grained streams.

1 Introduction

It is generally accepted that sediment supply is one of the most important parameters, which not only controls the mobility of the sediment in coarse-grained streams but also the channel form (Dade and Friend, 1998; Church, 2006). In particular, flume experiments (Dietrich et al., 1989) and numerical models (Wickert et al., 2013) have shown that a large sediment supply is commonly found in braided rivers where the material mobility is high, while a low sediment mobility is rather encountered in single-threat channels where the sediment supply is expected to be low. However, much less research has been conducted to investigate whether the granulometric composition, and particularly the sorting of the bed material, also exerts a measurable control on the mobility of coarse-grained material in streams. Here, we focus on this aspect and explore whether there is a link between the sorting of gravel bars, here expressed by the D_{96}/D_{50} ratios of the material, and the transport probability of individual clasts on these bars. We focus on gravelly streams in the Swiss Alps where artificial banks keep the flow in fixed, single-threat channels over several kilometres, and in the Peruvian Andes where streams are braided. We selected gravel bars close to water gauging stations, determined the grain size distribution of these bars and calculated the probability of sediment transport for a selected water runoff, which in our case corresponds to the mean annual water discharge Q_{mean} for comparison purposes. We explored whether these flows are strong enough to shift the D_{84} grain size, which is considered to build the sedimentary framework of gravel bars as recent flume experiments have shown (MacKenzi and Eaton, 2017;

MacKenzie et al., 2018). We thus considered the mobilization of the D_{84} grain size as a priori condition, and thus as a threshold, for a change in the sedimentary arrangement of the target gravels bars. The braided character of streams in Peru complicates the calculation of the sediment transport probability mainly because water flows in multiple active channels, and channel widths vary over short distances. For these streams, we selected reaches (c. 100 m long) where several active braided channels merge to a single one, before branching again. We are aware that this could eventually bias the results towards a greater material mobility, mainly because flows in single-threat segments are likely to have greater shear stresses than in braided reaches where the same water runoff is shared by multiple channels. The research sites thus offer conditions that are similar, or close, to a laboratory flume experiment (e.g., Dietrich et al., 1989) where channel gradients are nearly constant, and where sediment transport, conditioned by grain size specific thresholds, mainly depends on water runoff and channel widths, and therefore on the resulting flow strengths.

2 Methods and datasets

2.1 Entrainment of bedload material

Sediment mobilization is considered to occur when flow strength τ exceeds a grain size specific threshold τ_c (e.g., Paola et al., 1992):

$$\tau > \tau_c \quad (1).$$

We estimated the probabilities of $\tau > \tau_c$ for a given water discharge using a Monte Carlo modeling framework (see section 2.2). We conducted 10'000 simulations, and the results are reported as probability (or percentage) where $\tau > \tau_c$ during these iterations.

Threshold shear stress τ_c for the dislocation of grains with size D_x can be obtained using Shields (1936) criteria ϕ for the entrainment of sediment particles:

$$\tau_c = \phi(\rho_s - \rho) g D_x \quad (2),$$

where g denotes the gravitational acceleration, and ρ_s (2700 kg/m^s) and ρ the sediment and water densities, respectively. Among the various grain sizes, the 84th percentile D_{84} has been considered to best characterize the sedimentary framework of a gravel bar (Howard, 1980; Hey and Thorne, 1986; Grant et al., 1990). Accordingly, flows that dislocate the D_{84} grain size are strong enough to alter the gravel bar architecture (Grant et al., 1990). We acknowledge that many authors preferentially selected the D_{50} grain size as a threshold to quantify the minimum flow strengths τ_c to entrain the bed material (e.g., Paola and Mohrig, 1996; Pfeiffer and Finnegan, 2018). The selection of the D_{50} thus results in relatively low thresholds and in a greater entrainment probability. However, recent analogue experiments have shown that the coarse-grained trail of a material composition such as e.g., the D_{84} better characterizes the threshold conditions for the incipient motion of material on gravel bars than the D_{50} (MacKenzi and Eaton, 2017). We therefore followed the recommendations by MacKenzie et al. (2018) and selected the D_{84} grain size to quantify the threshold conditions in equation (2).

Bed shear stress τ is computed through (e.g., Tucker and Slingerland, 1997):

$$\tau = \rho g R S \quad (3).$$

Here, S denotes the energy gradient, and R is the hydraulic radius, which is approximated through water depth d where channel widths $W > 20 \times d$ (Tucker and Slingerland, 1997), which is the case here. The combination of expressions for: (i) the continuity of mass including flow velocity V, channel width W and water discharge Q:

$$Q = VWd \quad (4);$$

(ii) the relationship between flow velocity and channel bed roughness n (Manning, 1891):

$$V = \frac{1}{n} d^{2/3} S^{1/2} \quad (5);$$

and (iii) an equation for the Manning's roughness number n (Jarrett, 1984):

$$n = 0.32 S^{0.38} d^{-1/6} \quad (6);$$

yields a relationship where bed shear stress τ depends on gradient, water flux and channel width (Litty et al., 2017):

$$\tau = 0.54 \rho g \left(\frac{Q}{W} \right)^{0.55} S^{0.935} \quad (7).$$

This equation is similar to the expression by Hancock and Anderson (2002), Norton et al. (2016) and Wickert and Schildgen (2019) with minor differences regarding the exponent on the channel gradient S and on the ratio Q/W. These mainly base on the different ways of how bed roughness is considered. Note that this equation does not consider a roughness length scale (both vertical and horizontal) because we have no constraints on this variable.

We explored whether equation (2) could be solved using the Darcy-Weisbach friction factor f instead of Manning's n. According to Ferguson (2007), the friction factor f varies considerably between shallow- and deep-water flows and depends on grain size D_x relative to water depth d, and thus on the relative roughness. Ferguson (2007) developed a solution referred to as the Variable Power Equation (VPE), which accounts for the dependency of f on the relative importance of roughness-layer versus skin friction effects and thus on the D_x/d ratios. Calculations where the VPE was employed indeed revealed that roughness-layer effects have an impact on flow regimes where $D_{84}/d>0.2$ (Schlunegger and Garefalakis, 2018), which is likely to be the case in our streams. However, similar to Litty et al. (2016), we are faced with the problem that we have not sufficient constraints to analytically solve equation (2) with the VPE. We therefore selected Mannings's n instead, which allowed us to solve equation (2) analytically. But we acknowledge that this might introduce a bias.

2.2 *Monte Carlo simulations*

Predictions of sediment transport probability are calculated using Monte Carlo simulations performed within a MATLAB computing environment. All variables that are considered for the calculations of both sheer and critical sheer stresses (equations 7 and 2, respectively) are randomly selected within their possible ranges of variation (see next sections and Table 1). Except for the Shields ϕ variable that we consider to follow a uniform distribution between 0.03 and 0.06 (see section 2.3.1 for justification), we infer that all other variables follow a normal distribution, defined by its mean and one standard deviation. To ensure that no negative values introduce a bias to these iterations, only strictly positive values for channel widths and gradients are considered. In the case of water discharge, both null and positive values are kept for further calculations. Values excluded from the calculations, i.e. returning negative water discharge or null or negative channel width / slope gradient, yield "NaN" in the resulting vector. For each of the 10'000 iterations τ and τ_c are compared, which yields either "1" ($\tau > \tau_c$) or "0" ($\tau \leq \tau_c$). The sediment transport probability is then calculated as the sum of ones divided by the number of draws, from which the number of "NaN" values was subtracted before. Note that <2500 "NaN" were obtained for Rio Chico (PRC-ME17), which we mainly explain by the c. 150% relative standard deviation of the mean annual water discharge estimated for that river.

2.3 Parameters, datasets, uncertainties and sensitivity analysis

2.3.1 Shields variable ϕ

Assignments of values to ϕ vary and diverge between flume experiments (e.g., Carling et al., 1992; Ferguson, 2012; Powell et al., 2016) and field observations (Mueller et al., 2005; Lamb et al., 2008). Here, we considered that at the incipient motion of the D_{84}, the Shields variable ϕ is equally distributed between 0.03 and 0.06 (Dade and Friend, 1998) during the 10'000 iterations. However, based on a compilation of ϕ-values that were derived from field investigations and flume experiments, Lamb et al. (2008) revealed that ϕ is likely to depend on the energy gradient itself, where

$$\theta = 0.15 S^{0.25} \quad (8).$$

We refrain from using a slope dependency of ϕ at this stage for three major reasons: First, the consideration of equally distributed ϕ-values, in the range between 0.03 and 0.06, includes the Shields values of most field investigations and flume experiments where channel gradients were between 0.001 and 0.02 (spread of energy gradients of our streams, Table 1), as Lamb et al. (2008) and Bunte et al. (2013) have shown in their compilations. Second, ϕ-values show a large scatter in their slope-dependencies (Lamb et al., 2008). Accordingly, the consideration of equally distributed ϕ-values within a given range better complies with the large variability in ϕ–values that are commonly encountered in experiments and field surveys (Lamb et al., 2008). Third, the selected range considers most of the complexities that are related to the hiding of small clasts and the protrusion of large constituents (Buffington et al, 1992; Buffington and Montgomery, 1997;

Kirchner et al., 1990; Johnston et al., 1998), which, in turn, results in a large scatter of ϕ-values. In this context, Turowski et al. (2011) reported a larger variation in the threshold conditions for the mobilization of clasts than employed here. However, their streams have energy gradients between 0.06 and 0.1, with the consequence that some of the material is entrained during torrential floods where entrainment mechanisms are different. Finally, the selected ϕ-range also includes the hydrological conditions of channel forming floods where thresholds for the evacuation of sediment may be up to 1.2 times larger than for the incipient motion of individual clasts (Parker, 1978; Philips and Jerolmack, 2016; 2019; Pfeiffer et al., 2017). For instance, a 1.2- times larger threshold will increase the commonly employed ϕ value of 0.047 (Meyer-Peter and Müller, 1948), or alternatively 0.0495 (Wong and Parker, 2006), to the range between 0.036 and 0.0594, which is considered in the brackets of 0.03 and 0.06 that we employed in this paper. In summary, we consider that the selection of equally distributed ϕ-values between 0.03 and 0.06 does the best job to account for the large variability in ϕ–values that are commonly encountered in experiments and field surveys where energy gradients were between 0.001 and 0.02 (Lamb et al., 2008).

2.3.2 Grain size data

We collected grain size data from streams where water discharge has been monitored during the past decades. These are the Kander, Lütschine, Rhein, Sarine, Simme, Sitter and Thur Rivers in the Swiss Alps (Fig. 1a). The target gravel bars are situated close to a water gauging station. At these sites, 5 to 6 digital photographs were taken with a Canon EOS PR. The photos covered the entire lengths of these bars. A meter stick was placed on the ground and photographed together with the grains. Grain sizes were then measured with the Wolman (1954) method using the free software package ImageJ 1.52n (https://imagej.nih.gov). Following Wolman (1954), we used intersecting points of a grid to randomly select the grains to measure. A digital grid of 20x20 cm was calibrated with the meter stick on each photo. The size of the grid was selected so that the spacing between intersecting points was larger than the *b*-axis of most of the largest clasts (Table 1, Supplement S1). The grid was then placed on the photograph with its origin at the lower left corner of the photo. The intermediate or *b*-axis of approximately 250 – 300 grains (c. 50 grains per photo; Supplement S1) underneath a grid point was measured for each gravel bar. In this context, we inferred that the shortest (*c*-axis) was vertically oriented, and that the photos displayed the *a*- and *b*-axis only. In cases where more than half of the grain was buried, the neighboring grain was measured instead. In the few cases where the same grain lay beneath several grid points, then the grain was only measured once. Only grains larger than a few millimeters (>4-5 mm, depending on the quality of the photos) could be measured. While the limitation to precisely measure the finest-grained particles potentially biases the determination of the D_{50}, it will not influence the measurements of the D_{84} and D_{96} grain sizes, as the comparison between sieving and measuring of grains with the Wolman (1954) method has disclosed (Watkins et al., 2020). In addition, as will be shown below, the consideration of the

D_{96}/D_{84} instead of the D_{96}/D_{50} ratios yields a similar positive relationship to the mobility of grains. We complemented the grain size data sets with published information on the D_{50}, D_{84} and D_{96} grain size (Litty and Schlunegger, 2017; Litty et al., 2017) for further streams in Switzerland and Peru (Figs. 1a and 1b; Table 1). For a few streams in Switzerland, Hauser (2018) presented D_{84} grain size data from the same gravel bars as Litty and Schlunegger (2017), but the photo was taken one year later and possibly from a different site. For these 5 locations, we took the arithmetic mean of both surveys (Table 1, data marked with three asterisks). All authors used the same approach upon collecting grain size data, which justifies the combination of the new with the published datasets.

We finally assigned an uncertainty of 20% to the D_{84} threshold grain size, which considers the variability of the D_{84} within a gravel bar as the analysis of the intra-bar variation of the D_{84} for selected gravel bars in Switzerland shows (Supplement S1). The assignment of a 20% uncertainty to the D_{84} threshold grain size also considers a possible bias that could be related to the grain size measuring technique (e.g., sieving in the field versus grain size measurements using the Wolman method; Watkins et al., 2020). However, it is likely to underestimate the temporal variability in the grain size data, as a repeated measurement on some gravel bars in Switzerland has suggested (Hauser, 2018), but this aspect warrants further research.

2.3.3 Water discharge data

The Federal Office for the Environment (FOEN) of Switzerland has measured the runoff values of Swiss streams over several decades. We employed the mean annual discharge values over 20 years for these streams (Supplement S2) and calculated one standard deviation thereof (see Table 1). For the Peruvian streams, we used the mean annual water discharge values Q_{mean} reported by Litty et al. (2017) and Reber et al. (2017). These authors obtained the mean annual water discharge (Table 1) through a combination of hydrological data reported by the Sistema Nacional de Información de Recursos Hídricos and the TRMM-V6.3B43.2 precipitation database (Huffman et al., 2007). They also considered the intra-annual runoff variability as one standard deviation from Q_{mean} to account for the strong seasonality in runoff for the Peruvian streams, which we employed in this paper. For the Peruvian streams, the assigned uncertainties to Q_{mean} are therefore significantly larger than for the Swiss rivers (Table 1). A re-assessment of the inter-annual variability of water discharge for those streams in Peru where the gauging sites are close to the grain size sampling location (distance of a few kilometers) yields a one standard deviation of c. 50%, which is still much larger than for the Swiss rivers (Appendix S2). We therefore run sensitivity tests where we considered scenarios with different relative values for 1σ standard deviations of Q_{mean}.

We additionally ran sensitivity tests to explore how the mobility probability changes if runoff quantiles instead of Q_{mean} are considered (Supplement S3). In particular, we ran a series of Monte Carlo simulations for various runoff quantiles and then calculated the resulting probability of sediment mobilization for each of these quantiles. We then multiplied the occurrence probability of each runoff quantiles (listed by the Swiss authorities and calculated for the Peruvian streams based on 4 to 98-years equivalent daily records) with the corresponding transport probability and summed the values. This integration provides an alternative and more realistic estimate of transport probability (Supplement S3).

2.3.4 Channel width data

For the Swiss streams, channel widths and gradients (Table 1, Supplement S4) were measured on orthophotos and LiDAR DEMs with a 2-m resolution provided by Swisstopo. From this database, gradients were measured over a reach of c. 250 to 500 m. All selected Swiss rivers are single-thread streams following the classification scheme of Eaton et al. (2010), and flows are constrained by artificial banks where channel widths are constant over several kilometers. For these streams, we therefore measured the cross-sectional widths between the channel banks, similar to Litty and Schlunegger (2017).

We complemented this information with channel width (wetted perimeter) and energy gradient data for 21 Peruvian streams that were collected by Litty et al. (2017) in the field and on orthophotos taken between March-June. This period also corresponds to the season when the digital photos for the grain size analysis were made (Mai 2015). We acknowledge that widths of active channels in Peru vary greatly on an annual basis because of the strong seasonality of runoff (see above and large intra-annual variability of runoff in Table 1). We therefore considered scenarios where channel widths are twice as large as those reported on Table 1 (see Supplement S5).

The uncertainties on slope and channel width largely depend on the resolution of the digital elevation models underlying the orthophotos (2-m LiDAR DEM for Switzerland, and 30-m ASTER DEM for Peru). It is not possible to precisely determine the uncertainties on the slope values. Nevertheless, we anticipate that these will be smaller for the Swiss rivers than for the Peruvian streams mainly because of the higher resolution of the DEM. We ran sensitivity models where we explored how the probability of material transport changes in the Swiss rivers for various uncertainties on channel widths, energy gradients and mean annual discharge values (Supplement S4)

3 Results

The grain sizes range from 8 mm to 70 mm for the D_{50}, 29 mm to 128 mm for the D_{84}, and 52 mm and 263 mm to the D_{96}. The smallest and largest D_{50} values were determined for the Maggia and Rhein Rivers in the Swiss Alps, respectively (Table 1). The grain sizes in the Swiss Rivers also reveal the largest spread where the ratio between the D_{96} and D_{50} grain size ranges between 2.2 (Sarine) and 17.7 (Maggia Losone I), while the corresponding ratios in the Peruvian streams are between 2.1 (PRC-ME9) and 5.8 (PRC-ME17). In the Swiss Alps, the critical shear stresses τ_c (median values) for entraining the D_{84} grain size ranges from c. 20 Pa (Emme River) to c. 90 Pa (Rhein and Simme Rivers). In the Peruvian Andes, the largest critical shear values are <80 Pa (PRC-ME39). The shear stress values related to the mean annual water discharge Q_{mean} range from c. 15 Pa to 100 Pa in the Alps and from 20 Pa to >400 Pa in the Andes. Considering the strength of a mean annual flow and the D_{84} grain size as threshold, the probability of sediment transport occurrence in the Peruvian Andes and in the Swiss Alps comprises the full range between 0% and 100%.

Rivers that are not affected by recurrent high magnitude events (e.g., debris flows) and where the grain size distribution is not perturbed by lateral material supply are expected to display a self-similar grain size distribution (Whittaker et al., 2011; D'Arcy et al., 2017; Harries et al., 2018), characterized by a linear relationship between the D_{84}/D_{50} and D_{96}/D_{50} ratios. In case of the Maggia River, the largest grains are oversized if the D_{50} and the grain size distribution of the other streams are considered as reference (Fig. 2). This could reflect a response to the supply of coarse-grained material by a tributary stream where the confluence is <1 km upstream of the Maggia sites. Alternatively, and possibly more likely, it reflects the response to the high magnitude floods in this stream (Brönnimann et al., 2018). In particular, while the ratio between the last and first quantiles is <150 in the Swiss streams on the northern side the Alps, the ratio is 860 in the Maggia River. Interestingly, such ratios are not rare in Peru. However, we anticipate that the Peruvian streams are capable to accommodate such large runoff variabilities through much wider channel belts that are not confined by artificial banks along most of the streams. If we exclude the Maggia dataset, then the probability of sediment transport occurrence scales positively and linearly with the D_{96}/D_{50} ratios (Fig. 3A). The observed relationship appears stronger for the Swiss rivers (R^2 = 0.74, p-value = 2E-4) than for the Peruvian stream (R^2 = 0.33, p-value = 4E-3). These correlations suggest that gravel bars with a poorer sorting of the bed material, here expressed by a high D_{96}/D_{50} ratio, have a greater probability for the occurrence of sediment transport than those with better-sorted material. If the normalized residuals are plotted against the sorting, then they do not show any specific and significant patterns, and therefore appear independent of the sorting (Fig. 3B). This suggests that the inferred linear relationships between the probability of transport occurrence and the D_{96}/D_{50} are statistically robust. Although Fig. 3A suggests that the regression for the Swiss rivers (slope= 0.16±0.06; intercept= -0.34±0.31) differs from that of the Peruvian streams (slope= 0.18±0.11; intercept= -0.02±0.46), the regression parameters do not significantly differ when considering them within their 95% confidence intervals.

The use of discharge quantiles yields sediment transport probabilities within a large range between <10% and >50%, and they are higher than reported values from other streams (Torizzo and Pitlick, 2004; Pfeiffer and Finnegan, 2008). Additionally, the resulting probabilities are positively and linearly correlated with the probability of transport estimated with Q_{mean} (Figure S3 in Supplement), and the correlations are very similar between the Swiss (slope: 0.74±0.02; intercept: 0.05±0.01) and

Peruvian streams (slope: 0.73±0.19; intercept: 0.03±0.14). The mean annual discharge estimates Q_{mean} are likely biased by infrequent, but large magnitude floods, which could explain the 25% larger transport probabilities if Q_{mean} is used as reference runoff.

The assignments of different uncertainties on reach slopes, channel widths and discharge has no major influence on the inferred relationships between transport probability and sorting (Supplement S4, S5). For the Peruvian streams, however, assignments of twofold larger values to channel widths will decrease the probability of transport for a given sorting by c. 10-15%. The inferred linear relationship between both variables, however, will remain (Supplement S5).

4 Discussion and Conclusions

The sediment transport calculation is based on the inference that water discharge is strong enough to entrain the frame building grain size D_{84}. Therefore, the relationships between the mobilization probability and the D_{96}/D_{50} ratio could depend on the selected grain size percentile (e.g., the D_{84} versus the D_{50}), which sets the transport threshold. However, recent experiments have shown that the D_{84} better characterizes the thresholds for sediment entrainment than the D_{50} (MacKenzie et al. (2018). Besides, grain size D linearly propagates into the equation (2) and thus into the probability of $\tau > \tau_c$. Therefore, although the resulting probabilities vary depending on the threshold grain size, the relationships between the D_{96}/D_{50} ratio and the mobilization probability will not change. In addition, because of the linear relationship between the D_{84}/D_{50} and D_{96}/D_{50} ratios (Fig. 2), the same dependency of transport probability on sorting will also emerge if the D_{96}/D_{84} ratios are used. For the case where different discharge estimates are considered, here expressed as the ratio Δ of a specific runoff to the mean annual discharge Q_{meam}, then the corresponding probability of sediment transport will change by $\sim\sqrt{\Delta}$ (equation 7), but the dependency on the D_{96}/D_{50} ratio will remain. This is also valid if transport probabilities are calculated based on discharge quantiles (Supplement S3), and if larger channel widths particularly for Peruvian streams are considered (Supplement S5). This suggests that the sorting of the bed material has a measurable impact on the mobility of gravel bars and thus on the frequency of sediment mobilization irrespective of the selection of a threshold grain size and the choice of a reference water discharge. We note that while the data is relatively scarce and scattered (i.e., the same transport probability for a c. twofold difference in the D_{96}/D_{50} ratio), the relationships observed between the probability of transport occurrence and the degree of material sorting are significant with p-values <<0.01. We explain the scatter in the data by the natural stochastic nature of processes that are commonly encountered in the field.

For a given D_{96}/D_{50} ratio, the probability of material transport tends to be greater in the Peruvian than in the Swiss rivers (Fig. 3A). We explain the albeit small divergence in the transport probability between both settings (i.e. regression parameters overlap within their 95% confidence interval) by (i) the differences between the geomorphic conditions and sediment supply processes in both mountain ranges, (ii) the anthropogenic corrections of the Swiss streams, and (iii) the generally stochastic nature in sediment supply. In the Swiss Alps, the channel network, the processes on the hillslopes, and the pattern of erosion and sediment supply has mainly been conditioned, and thus controlled, by the glacial impact on the landscape and the large variability of exposed bedrock lithologies (e.g., Salcher et al., 2014; Stutenbecker et al., 2016). In addition, the intra-annual runoff variability is much lower than in the Peruvian streams (Supplement S2). In contrast, the erosion and sediment supply in the western Peruvian Andes is mainly driven by the combined effect of orographic rain (Montgomery et al., 2001; Viveen et al., 2019) and earthquakes (McPhilips et al., 2014), and the intra-annual runoff variability is quite large (Table 1). Because the patterns, conditions and mechanisms of sediment supply largely influence the grain size distribution of the supplied material (Attal et al., 2015), and as consequence, the downstream propagation of these grain size signals (Sklar et al., 2006), we do not expect identical relationships between grain size parameters and probability of sediment transport in both mountain ranges. In the same sense, the large variability and stochastic nature of sediment supply and transport processes could also explain the large spread in transport probability that we report for the Swiss and Peruvian streams. A large spread in transport probability was also inferred for mountainous rivers in the USA (Torizzo and Pitlick, 2004; Pfeiffer and Finnegan, 2018). We note, however, that Pfeiffer and Finnegan (2018) report lower transport probabilities that range between 8% and nearly 100% for the West Coast, 1% and 12% for the Rocky Mountains, and <10% for the Appalachian Mountains. In a broader sense, these authors considered the ratio between sediment supply and sediment transport capacity as criteria for the incipient motion of bedload material, which differs from the mobility criteria that we set in this paper. However, the largest difference stems from the values of the database. While the D_{50} of Pfeiffer and Finnegan (2018) has nearly the same size as the D_{84} reported here, their channel gradients tend to be 3 times lower. Because shear stress linearly depends on gradient (equation 7), then the probability where $\tau > \tau_c$ will be directly and proportionally affected by this. Nevertheless, even if we would select a different channel gradient, the probability of material mobilization will go down (most likely linearly), but the dependency of the transport probability on the grain size sorting will remain. Accordingly, despite the large scatter in the dataset, the relationships between transport mobility and sorting is statistically significant with p-values <<0.01, which suggests the sorting of coarse-grained bed sediments has a measurable impact on the mobility of the bedload material. We therefore conclude that besides the generally accepted controls including transport regime and sediment supply (Dade and Friend, 1998; Church, 2006), the sorting of the bed material represents an additional, yet important variable that influences the mobility of material on gravel bars. In addition, further research could possibly disclose a mechanism where sediment supply, material sorting and transport probability may be closely linked through a positive feedback.

Figure 1

A) Map showing the sites where grain size data has been measured in the Swiss Alps. The research sites are close to water gauging stations; B) map showing locations for which grain size and water discharge data is available in Peru (Litty et al., 2017).

Figure 2

Relationship between ratio of the D_{96}/D_{50} and D_{84}/D_{50}, implying that the D_{96} grain sizes of the Maggia gravel bars are too large if the D_{50} is taken as reference and if the other gravel bars are considered.

Figure 3

A) Relationships between the probability of sediment transport occurrence and the D_{96}/D_{50} ratio, which we use as proxy for the sorting of the gravel bar, in the Swiss and Peruvian rivers. B) Normalized residuals that are plotted against the sorting. The normalized residuals do not show any specific and significant patterns.

Table 1

Channel morphometry (width and gradient), grain size and water discharge measured at the research sites. The table also shows the results of the various calculations (critical shear stress τ_c, shear stress τ of a flow with a mean annual runoff Q_{med}, and probability of sediment transport occurrence related to this flow).

Data availability

All data that have been used in this paper are listed in Table 1 and in the Supplement.

Author contributions

FS and RD designed the study. RD conducted the Monte Carlo Simulation. PG provided the grain size data in the Supplement. FS wrote the paper with input from RD and PG. All authors discussed the article.

Competing interests

The authors declare that they have no conflict of interest.

Acknowledgements

The Federal Office for the Environment (FOEN) is kindly acknowledged for providing runoff data for the Swiss streams. This research was supported by SNF (No. 155892).

References

Attal, M., Mudd, S.M., Hurst, M.D., Weinmann, B., Yoo, K., and Naylor, N.: Impact of change in erosion rate and landscape steepness on hillslopes and fluvial sediments grain size in the Feather River basin (Sierra Nevada, California), Earth Surf. Dyn., 3, 201-222, 2015.

Bunte, K., Abt, S.R., Swingle, K.W., Cenderelli, D.A., and Schneider, M.: Critical Shields values in coarse-bedded steep streams, Water Res. Res., 49, 7427-7447, 2013.

Brönnimann, S., et al.: 1968 – das Hochwasser, das die Schweiz veränderte. Ursachen, Folgen und Lehren für die Zunkunft, Geographica Bernensai, G94, 52 p., 2018

Buffington, J., Dietrich, W.E., and Kirchner, J.W., Friction angle measurements on a naturally formed gravel streambed: Implications for critical boundary shear stress, Water Res. Res., 28, 411-425, 1992.

Buffington, J. M. and Montgomery, D. R.: A systematic analysis of eight decades of incipient motion studies, with special reference to gravel-bedded rivers, Water Resour. Res., 33, 1993-2029, 1997.

Carling, P. A., Kelsey, A., and Glaister, M. S.: Effect of bed rough- ness, particle shape and orientation on initial motion criteria, in: Dynamics of gravel-bed rivers, edited by: Billi, P., Hey, R. D., Throne, C. R., and Tacconi, P., 23–39, John Wiley and Sons, Ltd., Chichester, 1992.

Church, M.: Bed material transport and the morphology of alluvial river channels, Ann. Rev. Earth Planet. Sci., 34, 325-354, 2006.

D'Arcy, M., Whittaker, A.C., and Roda-Bolduda, D.C.: Measuring alluvial fan sensitivity to past climate changes using a self-similarity approach to grain-size fining, Death Valley, California, Sedimentology, 64, 388-424, 2017.

Dade, B. and Friend, P.F.: Grain-size, sediment-transport regime, and channel slope in alluvial rivers, J. Geol., 106, 661-676, 1988.

Dietrich, W.E., Kirchner, J.W., Hiroshi, I., and Iseya, F.: Sediment supply and the development of the coarse surface layer in gravel-bedded rivers, Nature, 340, 215-217, 1989.

Eaton, B.C., Moore, R.D., and Giles, T.R.: Forest fire, bank strength and channel instability: the 'unusual' response of Fishtrap Creek, British Columbia, Earth Surf. Process. Landf., 35, 1167–1183, 2010.

Ferguson, R., Flow resistance equations for gravel- and boulder- bed streams. Water Resour. Res., 43, W05427, 2007.

Ferguson, R.: River channel slope, flow resistance, and gravel entrainment thresholds, Water Resources Research, 48, W05517, 2012.

Grant, G. E., Swanson, F. J., and Wolman, M. G.: Pattern and origin of stepped-bed morphology in high gradient streams, western Cascades, Oregon, GSA Bull., 102, 340–352, 1990.

Hancock, G.S., and Anderson, B.S.: Numerical modeling of fluvial strath-terrace formation in response to oscillating climate, GSA Bull., 9, 1131-1142, 2002.

Harries, R.M., Kirstein, L.A., Whittaker, A.C., Attal, M., Peralta, S., and Brooke, S.: Evidence for self-similar bedload transport on Andean alluvial fans, Iglesia, basin, South Central Argentina, J. Geophys. Res. - Earth Surface, 123, 2292-2315, 2018.

Hauser, R.: Abhängigkeit von Korngrössen und Flussformen in den Schweizer Alpen, Unpubl. Ms thesis, Univ. Bern, Bern, Switzerland, 64 p., 2018.

Hey, R. D. and Thorne, C. R.: Stable channels with mobile gravel beds, J. Hydrol. Eng., 112, 671–

689, 1986.

Howard, A. D.: Threshold in river regimes, in: Thresholds in geomorphology, edited by: Coates, D.R, and Vitek, J.D., Allen and Unwin, Boston, MA, 227-258, 1980.

Huffman, G. J., Adler, R. F., Bolvin, D. T., Gu, G., Nelkin, E. J., Bowman, K. P., and Wolff, D. B.: The TRMM multi-satellite precipitation analysis: Quasi-global, multi-year, combined-sensor precipitation esti- mates at fine scale, J. Hydromet., 8, 38–55, 2007.

Jarrett, R. D.: Hydraulics of high-gradient streams, J. Hydraul. Eng., 110, 1519-1939, 1984.

Johnston, C.E., Andrews, E.D., and Pitlick, J., In situ determination of particle friction angles of fluvial gravels, Water Resour. Res., 34, 2017-2030, 1998.

Kirchner, J.W., Dietrich, W.E., Iseya, F., and Ikeda, H.: The variability of critical shear stress, friction angle, and grain protrusion in water-worked sediments, Sedimentology, 37, 647-672, 1990.

Lamb, M. P., Dietrich, W. E., and Venditti, J. G.: Is the critical Shields stress for incipient sediment motion dependent on channel bed slope? J. Geophys. Res., 113, F02008, 2008.

Litty, C., Duller, R., Schlunegger, F., Paleohydraulic reconstruction of a 40 ka-old terrace sequence implies that water discharge was larger than today, Earth Surf. Proc. Landf., 41, 884-898, 2016.

Litty, C. and Schlunegger, F.: Controls on pebbles' size and shape in streams of the Swiss Alps, J. Geol., 125, 101-112, 2017.

Litty, C., Schlunegger, F., and Viveen, W.: Possible threshold controls on sediment grain properties of Peruvian coastal river basins, Earth Surf. Dyn., 5, 571-583, 2017.

MacKenzie, L. and Eaton, B.C.: Large grains matter: constraining bed stability and morphodynamics during two nearly identical experiments, Earth Surf. Proc. Landf., 42, 1287-1295, 2017.

MacKenzie, L., Eaton, B.C. and Church, M.: Breaking from the average: Why large grains matter in gravel-bed streams. Earth Surf. Proc. Landf., 43, 3190-3196, 2018.

Manning, R.: On the flow of water in open channels and pipes, Trans. Inst. Civil Eng. Ireland, 20, 161–207, 1891.

Meyer-Peter, E., and Müller, R., Formulas for bedload transport, Proceedings of the 2nd meeting of the Int. Assoc. Hydraul. Struct. Res., Stockholm, Sweden. Appendix 2, 39–64, 1948.

McPhilips, D., Bierman, P.R., and Rood, D.H.: 2014, Millennial-scale record of landslides in the Andes consistent with earthquake trigger, Nature Geosci., 7, 925-930, 2014.

Montgomery, D. R., Balco, G., and Willett, S. D.: Climate, tectonics, and the morphology of the Andes, Geology, 29, 579–582, 2001.

Mueller, E. R., Pitlick, J., and Nelson, J. M.: Variation in the reference Shields stress for bed load transport in gravel- bed streams and rivers, Water Res. Res., 41, W04006, 2005.

Norton, K.P., Schlunegger, F., and Litty, C.: On the potential for regolith control of fluvial terrace formation in semi-arid escarpments, Earth Surf. Dyn., 4, 147-157, 2016.

Paola, C., Heller, P.L., and Angevine, C.: The large-scale dyanmics of grain size variation in alluvial basins, 1: Theory, Basin Res., 4, 73-90, 1992.

Paola, C. and Mohring, D.: Palaeohydraulics revisted: palaeoslope estimation in coarse-grained braided rivers, Basin Res., 8, 243-254, 1996.

Parker, G., Self-formed straight rivers with equilibrium banks and mobile bed. Part 2. The gravel river, J. Fluid Mech., 89, 127-146, 1978. doi:10.1017/S0022112078002505.

Pfeiffer, A.M., Finnegan, N.J., and Willenbring, J.K., Sediment supply controls equilibrium channel geometry in gravel rivers, Proc. Natl. Acad. Sci. U.S.A., 114, 3346-3351, 2017.

Pfeiffer, A.M., and Finnegan, N.J.: Regional variation in gravel riverbed mobility, controlled by hydrological regime and sediment supply, Geophys. Res. Lett., 45, 3097-3106, 2018.

Philips, C.B., and Jerolmack, D.J., Self-organization of river channels as a critical filter on climate signals, Science, 352, 649-697, 2016.

Phillips, C.B., Jerolmack, D.J., Bankfull transport capacity and the threshold of motion in coarse-grained rivers, Water Res. Res., 55, 11316-11330, 2019.

Powell, M. D., Ockleford, A., Rice, S. P., Hillier, J. K., Nguyen, T., Reid, I., Tate, N. J., and Ackerley, D.: Structural properties of mobile armors formed at different flow strengths in gravel-bed rivers, J. Gephys. Res. – Earth Surface, 121, 1494-1515, 2016.

Reber, R., Delunel, R., Schlunegger, F., Litty, C., Madella, A., Akcar, N., and Christl, M.: Environmental controls on 10Be-based catchment-averaged denudation rates along the western margin of the Peruvian Andes, Terra Nova, 29, 282-293, 2017.

Turowski, J.M., Badoux, A., and Rickenmann, D., Start and end of bedload transport in gravel-bed streams, Geophys. Res. Lett., 38, L04401, 2011.

Salcher, B.C., Kober, F., Kissling, E., and Willett, S.D.: Glacial impact on short-wavelength topography and long-lasting effects on the denudation of a deglaciated mountain range, Global Planet. Change, 115, 59-70, 2014.

Schlunegger, F., and Garefalakis, P., Clast imbrication in coarse-grained mountain streams and stratigraphic archives as indicator of deposition in upper flow regime conditions, Earth Surf. Dyn., 6, 743-761.

Shields A.: Anwendung der Ahnlichkeitsmekanik und der Turbulenzforschung auf die Geschiebebewegung, Mitt. Preuss. Versuch. Wasserbau Schiffbau, 26 p., Berlin, 1936.

Sklar, L.S., Dietrich, W.E., Foufoula-Georgiou, E.F., Lashermes, B., and Bellugi, D.: 2006, Do gravel bed river size distributions record channel network structure?, Water Res. Res., 42, W06D18, 2006.

Stutenbecker, L., Costa, A., and Schlunegger, F.: Lithological control on the landscape form from the upper Rhône Basin, Central Swiss Alps, Earth Surf. Dyn., 4, 253-272, 2016.

Torizzo, M., and Pitlick, J.: Magnitude-frequency of bed load transport in mountain streams in Colorado, J. Hydrol., 290, 137-151.

Tucker, G., and Slingerland, R.: Drainage basin responses to climate change, Water Res. Res, 33,

2031-2047, 1997.
Viveen, W., Zellavos-Valdivia, L., and Sanjurjo-Sanchez, J.: The influence of centennial-scale variations in the South American summer monsoon and base-level fall on Holocene fluvial systems in the Peruvian Andes, Gobal Planet. Change, 176, 1.22, 2019.
Watkins, S., Whittaker, A.C., Bell, R.E., Brooke, S.A.S., Ganti, V., Gawthrope, R.L., McNeill, L.C., and Nixon, C.W.: Straight from the source's mouth: Controls on field-constrained sediment export across the entire active Corinth rift, central Creece, Basin Res., in press. Doi: 10.111/bre.12444.
Whittaker, A.C., Duller, R.A., Springett, J., Smithells, R.A., Whitchurch, A.L., and Allen, P.A.: Decoding downstream trends in straigraphic grain size as a function of tectonic subsidence and sediment supply, GSA Bull., 123, 1363-1382, 2011.
Wickert , A.D., Martin, J.M., Tal, M., Kim, W., Sheets, B., and Paola, C.: River channel lateral mobility: metrics, time scales, and controls, J. Geophys. Res. - Earth Surface, 118, 396-412, 2013.
Wickert, A.D., and Schildgen, T.F.: Long-profile evolution of transport-limited gravel-bed rivers, Earth Surf. Dyn, 7, 17-43, 2019.
Wolman, M. G.: A method of sampling coarse riverbed material, Eos Trans AGU, 35, 951-956, 1954.
Wong, M., and Parker, G., Reanalysis and correction of bed-load relation of Meyer-Peter and Müller using their own database, J. Hydraul. Eng., 132, 1159-1168, 2006.

TABLE 1. GRAIN SIZE, CHANNEL METRICS, SHEAR STRESSES AND RELATIVE TRANSPORT TIME

Id	River	Site coordinates Latitude (DD WGS84)	Site coordinates Longitude (DD WGS84)	Channel width along reach (m)	Reach gradient (m/m)	Qmean: Mean annual water discharge (m3/s)	Standard deviation of Qmean (m3/s)**	D50 (m)	D84 (m)	D96 (m)	D96/D50	D84/D50	Critical Sheer (median) (Pa)	Critical Sheer (16th%) (Pa)	Critical Sheer (84th%) (Pa)	Sheer stress in response to Qmean (median) (Pa)	Sheer stress in response to Qmean (16th%) (Pa)	Sheer stress in response to Qmean (84th%) (Pa)	Relative transport time for Qmean and the D84 as threshold
1	*Emme**	46.96	7.75	30	0.007	11.9	2.5	0.009	0.029	0.052	5.8	3.2	21	15	29	30	23	39	81%
2	*Landquart**	46.98	9.61	32	0.018	24.1	5.1	0.025	0.083***	0.135	5.4	3.3	60	42	82	102	79	130	90%
3	*Waldemme Littau**	47.07	8.28	27	0.011	15.5	2.8	0.009	0.050***	0.084	9.3	5.5	36	26	50	55	42	69	85%
4	*Reuss**	46.88	8.62	48	0.007	42.9	4.7	0.009	0.032***	0.064	7.2	4.1	27	19	37	48	38	60	93%
5	*Maggia Losone II**	46.17	8.77	84	0.005	22.7	10.8	0.011	0.046***	0.127	11.3	4.1	33	23	46	19	12	26	11%
6	*Maggia Losone I**	46.17	8.77	22	0.005	22.7	10.8	0.008	0.033***	0.140	17.7	4.1	24	17	33	39	26	53	83%
7	*Rhein*	47.01	9.30	92	0.002	167.5	24.5	0.070	0.128	0.169	2.4	1.8	92	65	127	26	20	32	0%
8	*Sarine*	46.36	7.05	24	0.004	21.0	3.9	0.049	0.080	0.108	2.2	1.6	58	41	80	27	21	35	4%
9	*Lütschine*	46.38	7.53	32	0.007	19.0	1.7	0.061	0.111	0.153	2.5	1.8	80	56	110	39	31	49	4%
10	*Thur*	47.30	9.12	52	0.002	37.9	6.8	0.024	0.045	0.069	2.9	1.8	32	23	45	13	10	17	2%
11	*Simme*	46.39	7.27	15	0.014	12.0	1.8	0.062	0.119	0.263	4.2	1.9	86	61	118	87	68	109	51%
12	*Sitter*	47.24	9.19	26	0.005	10.2	1.6	0.028	0.064	0.094	3.3	2.2	46	33	64	24	19	30	6%
13	*Kander*	46.39	7.40	26	0.009	20.0	2.3	0.054	0.116	0.193	3.6	2.1	84	59	115	58	46	72	19%
14	*Sense**	46.89	7.35	24	0.005	8.7	1.7	0.024	0.060	0.096	4.0	2.5	43	31	60	22	17	28	6%
15	PRC-ME1#	-18.12	-70.33	6	0.015	3.4	0.8	0.023	0.062	0.100	4.3	2.7	45	32	62	76	58	97	89%
16	PRC-ME3#	-17.82	-70.51	6	0.013	4.0	5.0	0.025	0.055	0.110	4.4	2.2	40	28	55	83	46	126	86%
17	PRC-ME5#	-17.29	-70.99	7	0.018	3.4	1.0	0.026	0.051	0.078	3.0	2.0	37	26	51	82	61	107	96%
18	PRC-ME6#	-17.03	-71.69	26	0.051****	38.1	37.8	0.015	0.036	0.075	5.0	2.4	26	18	36	432	244	643	100%****
19	PRC-ME802#	-16.34	-72.13	15	0.019	30.1	21.7	0.020	0.060	0.100	5.0	3.0	43	31	60	193	116	278	98%
20	PRC-ME7#	-16.51	-72.64	100	0.005	68.4	52.7	0.052	0.087	0.120	2.3	1.7	63	44	86	31	18	45	8%
21	PRC-ME9#	-16.42	-73.12	70	0.004	91.1	82.2	0.048	0.068	0.100	2.1	1.4	49	35	68	37	21	54	29%
22	PRC-ME1402#	-15.85	-74.26	3	0.014	20.4	29.9	0.013	0.030	0.060	4.6	2.3	22	15	30	336	182	510	100%
23	PRC-ME15#	-15.63	-74.64	23	0.003	12.1	16.7	0.029	0.064	0.096	3.3	2.2	46	33	64	19	10	29	5%
24	PRC-ME16#	-13.73	-75.89	20	0.013	13.6	17.8	0.030	0.066	0.130	4.3	2.2	48	34	66	85	47	129	80%
25	PRC-ME17#	-13.47	-76.14	5	0.010	10.1	14.8	0.013	0.038	0.076	5.8	2.9	28	19	38	126	68	191	97%
26	PRC-ME19#	-13.12	-76.39	60	0.010	26.4	25.9	0.020	0.046	0.088	4.4	2.3	33	23	46	49	28	72	72%
27	PRC-ME20#	-12.67	-76.65	22	0.008	8.2	9.8	0.016	0.048	0.088	5.5	3.0	35	25	48	38	21	57	55%
28	PRC-ME22#	-12.25	-76.89	5	0.022	3.7	4.3	0.030	0.050	0.088	2.9	1.7	36	26	50	141	78	212	96%
29	PRC-ME39#	-11.79	-76.99	40	0.018	4.9	5.1	0.053	0.105	0.150	2.8	2.0	76	54	104	42	24	63	13%
30	PRC-ME23#	-11.61	-77.24	20	0.010	8.9	7.8	0.055	0.083	0.120	2.2	1.5	60	42	82	48	27	70	32%
31	PRC-ME25#	-11.07	-77.59	5	0.012	3.8	4.6	0.028	0.077	0.130	4.6	2.8	56	39	77	82	45	124	72%
32	PAT-ME#	-10.72	-77.77	30	0.014	30.9	24.3	0.018	0.036	0.060	3.3	2.0	26	18	36	102	60	148	97%
33	PRC-ME38#	-10.07	-78.16	15	0.004	9.8	12.7	0.017	0.034	0.052	3.1	2.0	25	17	34	28	15	42	56%
34	PRC-ME27#	-8.97	-78.62	40	0.005	96.1	67.7	0.020	0.054	0.090	4.5	2.7	39	27	54	61	37	87	77%
35	PRC-ME30#	-7.32	-79.48	40	0.007	25.4	27.7	0.029	0.063	0.100	3.4	2.2	45	32	63	44	24	65	46%

Italic=Swiss Rivers, plain=Peruvian Rivers

Water discharge data from the Swiss Rivers is taken from the Swiss Federal Office for the Environment (FOEN: www. hydrodaten.admin.ch). Reported values represent discharges monitored over the period 1990-2011; Except for the Rhein (1977-1990).

Water discharge and drainage basin size data from the Peruvian Rivers is taken from Reber et al. (2017) and Litty et al. (2017)

#The grain size data from the Peruvian streams is taken from Litty et al. (2017)

*The grain size data, channel width and gradient data from the Emme, Landquart, Reuss, Maggia and Sense Rivers is taken from Litty and Schlunegger (2017)

**While standard deviation on annual water flow represents inter-annual variance for Switzerland, it represents intra-annual ones in Peru.

***Mean values of measurement results by Hauser (2017) and Litty and Schlunegger (2017)

****The results are possibly biased by an error on the slope, which appears too steep; the consideration of a flatter slope (0.013) still yields 99%

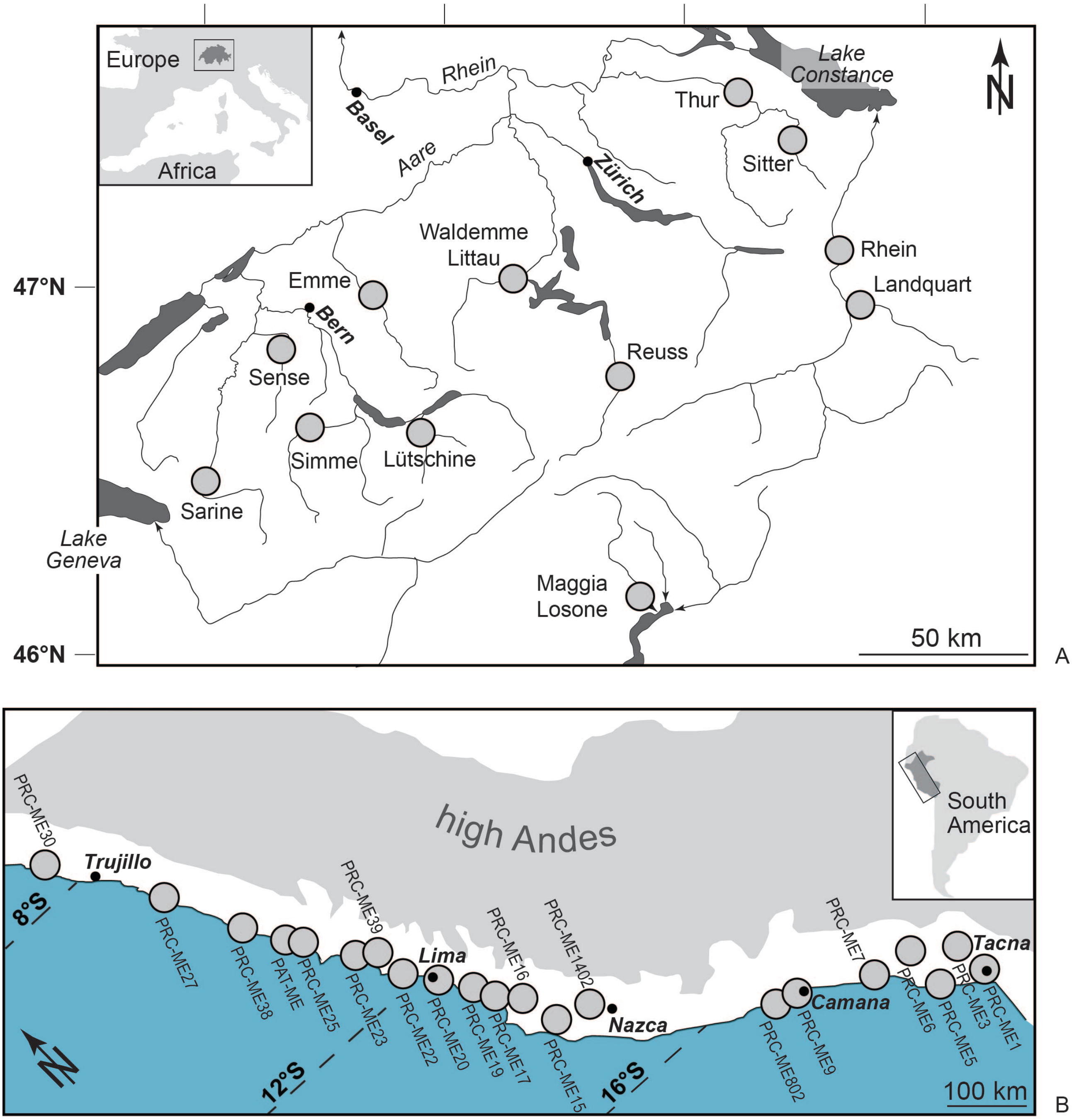
Europe
Africa
Rhein
Basel
Aare
Zürich
Lake Constance
Thur
Sitter
Waldemme
Littau
Rhein
Landquart
47°N
Emme
Bern
Sense
Reuss
Simme
Lütschine
Sarine
Lake Geneva
Maggia
Losone
46°N
50 km
A
high Andes
South America
PRC-ME30
Trujillo
8°S
PRC-ME27
PRC-ME38
PAT-ME
PRC-ME25
PRC-ME39
PRC-ME23
PRC-ME22
Lima
PRC-ME20
PRC-ME19
PRC-ME16
PRC-ME17
PRC-ME1402
PRC-ME15
Nazca
12°S
16°S
PRC-ME802
PRC-ME9
Camana
PRC-ME7
PRC-ME6
PRC-ME5
PRC-ME3
Tacna
PRC-ME1
100 km
B

Figure 1

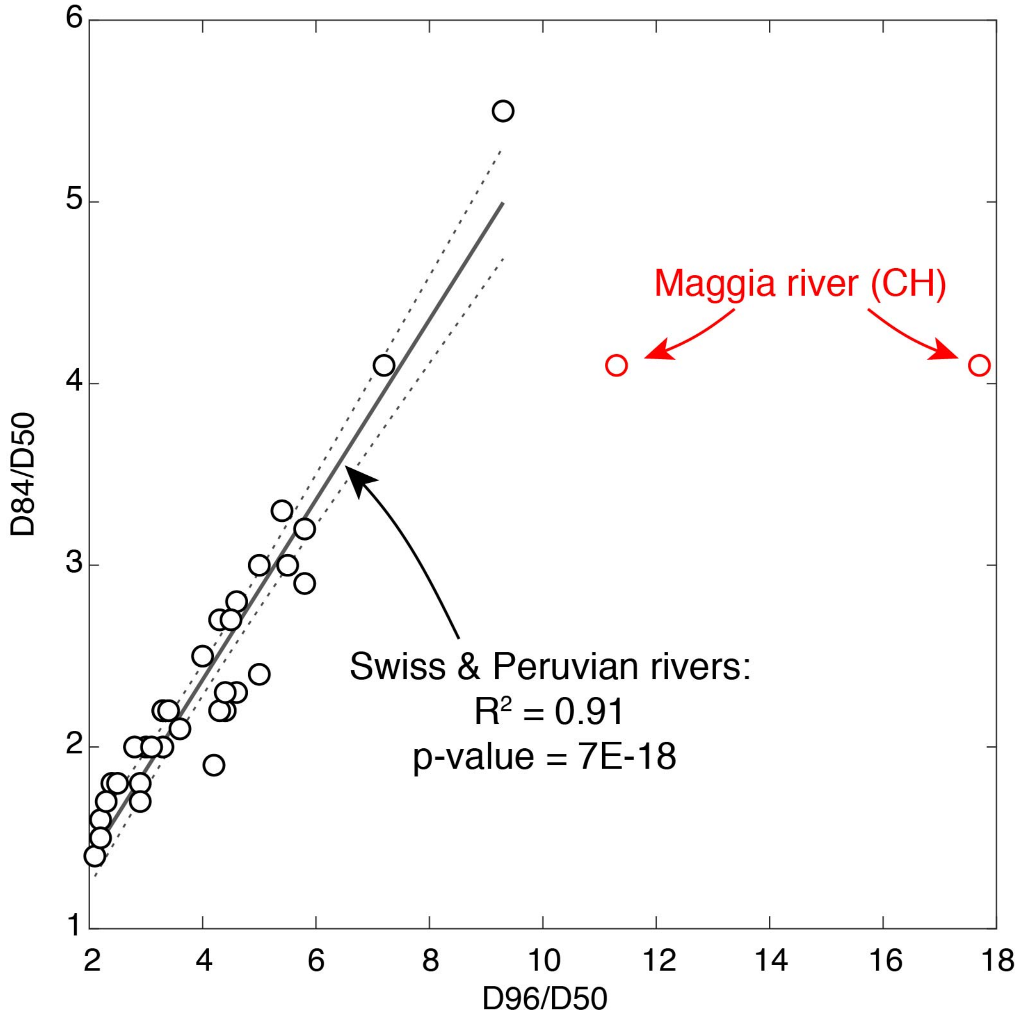
Maggia river (CH)
Swiss & Peruvian rivers:
$R^2 = 0.91$
p-value = 7E-18
D84/D50
D96/D50

Figure 2

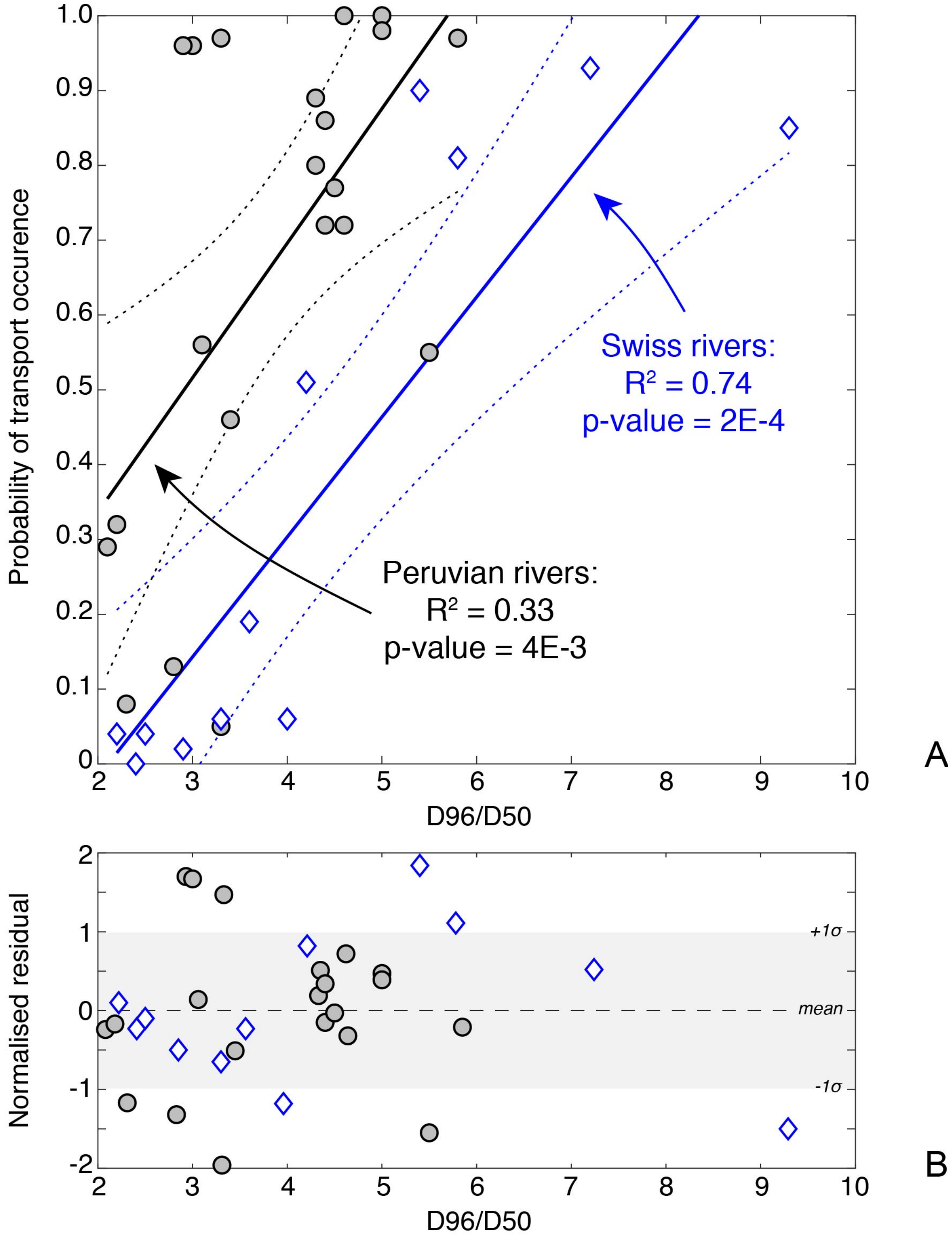

Probability of transport occurence
D96/D50
Swiss rivers:
R^2 = 0.74
p-value = 2E-4
Peruvian rivers:
R^2 = 0.33
p-value = 4E-3
A
Normalised residual
+1σ
mean
-1σ
B

557

Figure 3